# Spectral Mixture Modeling with Laboratory Near-Infrared Data I: Insights into Compositional Analysis of Europa

A. Emran[a]

[a]*NASA Jet Propulsion Laboratory, California Institute of Technology, Pasadena, 91109, CA, USA*

**Abstract**

Europa's surface composition and physical characteristics are commonly constrained using spectral deconvolution through linear mixture (LM) modeling and radiative transfer–based (RT) intimate mixture modeling. Here, I compared the results of these two spectral modeling— LM versus RT— against laboratory spectra of water ($H_2O$) ice and sulfuric acid octahydrate (SAO; $H_2SO_4{\cdot}8H_2O$) mixtures measured at near-infrared wavelengths ($\sim$1.2–2.5 $\mu$m) with grain sizes of 90–106 $\mu$m (Hayes and Li, 2025). The modeled abundances indicate that the RT more closely reproduces the laboratory abundances, with deviations within $\pm$5% for both $H_2O$ ice and $H_2SO_4{\cdot}8H_2O$ with $\sim$100 $\mu$m grains. In contrast, the LM shows slightly larger discrepancies, typically ranging from $\pm$5-15% from the true abundances. Interestingly, both LM and RT tend to consistently overestimate the abundance of $H_2SO_4{\cdot}8H_2O$ and underestimate $H_2O$ ice across all mixtures. Nonetheless, when $H_2SO_4{\cdot}8H_2O$ either dominates ($>$ 80% as observed on Europa's trailing hemisphere; Carlson et al., 2005) or is present only in trace amounts ($\sim$10% on areas in Europa's leading hemisphere; Dalton III et al., 2013; Ligier et al., 2016), both the LM and RT render acceptable results within $\pm$10% uncertainty. Thus, spectral modeling using the RT is preferred for constraining the surface composition across Europa, although the LM remains viable in specific compositional regimes.

*Keywords:* Spectral modeling, Radiative transfer, Europa, Icy moon, Surface composition, Planetary science

## 1. Introduction

Estimations of planetary surface composition—on both terrestrial and icy bodies—across the Solar System are done using spectral deconvolution via linear mixture (LM) modeling and radiative transfer (RT) theory, known as intimate mixture modeling (e.g., Li and Li, 2011; Dalton III et al., 2012; Li and Milliken, 2015; Goudge et al., 2015; Shirley et al., 2016; Liu et al., 2016; Emran et al., 2021; Emran and Stack, 2025; Emran, 2025a). In linear mixture modeling, also commonly known as the areal mixture approach, the reflectance of a mixture is represented as a linear combination of the spectra of its

*Email address:* `al.emran@jpl.nasa.gov` (A. Emran)

constituent materials, assuming that each material exists in spatially distinct patches (e.g., Hapke, 2012; Dalton III et al., 2012; Emran et al., 2023; Stack and Milliken, 2015). In contrast, radiative transfer-based intimate mixture modeling assumes that the component materials are physically mixed in a "salt-and-pepper" fashion, resulting in a nonlinear combination of the reflectance spectra of the constituents (e.g., Mustard and Pieters, 1987; Poulet and Erard, 2004; Li and Li, 2011; Hapke, 2012; Li and Milliken, 2015). In planetary science, Hapke's radiative transfer model Hapke (1981, 2001, 2012) has been extensively applied for spectral modeling to constrain the compositions of icy bodies in the outer Solar System (refer to Emran and Chevrier, 2022, 2023; Khuller and Emran, 2025, for exhaustive references).

Although both the LM and RT spectral modeling have their inherent advantages and limitations (e.g., Keshava and Mustard, 2002; Hapke, 2012), they have been successfully applied to constrain the surface composition of Europa (e.g., Shirley et al., 2016). Using data from both ground- and space-based observations, Europa's surface composition has been derived from visible and near-infrared (VIS-NIR) wavelengths using the LM modeling (e.g., Dalton III, 2007; Dalton III et al., 2012; Shirley et al., 2010; Brown and Hand, 2013; Ligier et al., 2016; Davis and Brown, 2024; Emran, 2025a) and the RT modeling based on Hapke (1981) theory (e.g., Carlson et al., 2005; Mishra et al., 2021; Mermy et al., 2023). While a variety of ice and non-ice components have been hypothesized on Europa's surface, water ($H_2O$) ice and sulfuric acid octahydrate (SAO; $H_2SO_4{\cdot}8H_2O$) have consistently been identified as the major constituents using both the LM and RT modeling approaches, as well as by comparisons with laboratory spectra (e.g., Moroz, 1966; Pilcher et al., 1972; Carlson et al., 1999a, 2005; Dalton III, 2007; Dalton III et al., 2012; Shirley et al., 2010, 2016; Ligier et al., 2016; Mermy et al., 2023; Emran, 2025a).

Nonetheless, evaluating the accuracy of the LM and RT modeling in constraining surface composition remains a critical area of research for accurately understanding Europa's surface and interpreting its geology. Shirley et al. (2016) compared abundance estimates derived from the LM and RT modeling using data from the Galileo Near-Infrared Mapping Spectrometer (NIMS; Carlson et al., 1992). Their analysis of spectra from various regions on Europa revealed that both approaches rendered consistent results, with linear correlation coefficients of $\geq 0.98$ for $H_2O$ ice and $H_2SO_4{\cdot}8H_2O$ abundances by both models (Shirley et al., 2016). However, until this current study, validation of these mixture modeling using laboratory data has remained lacking. Recently, Hayes and Li (2025) measured reflectance spectra of $H_2O$ ice and $H_2SO_4{\cdot}8H_2O$ mixtures at varying ratios relevant to Europa— offering a unique opportunity to assess spectral modeling accuracy. In this study, as part of a series of investigations (Emran, 2025b), I assess the accuracy of the LM and RT modeling against the laboratory spectra of $H_2O$ ice and $H_2SO_4{\cdot}8H_2O$ mixtures at near-infrared (NIR) wavelengths— providing a framework for quantitatively constraining Europa's surface composition.

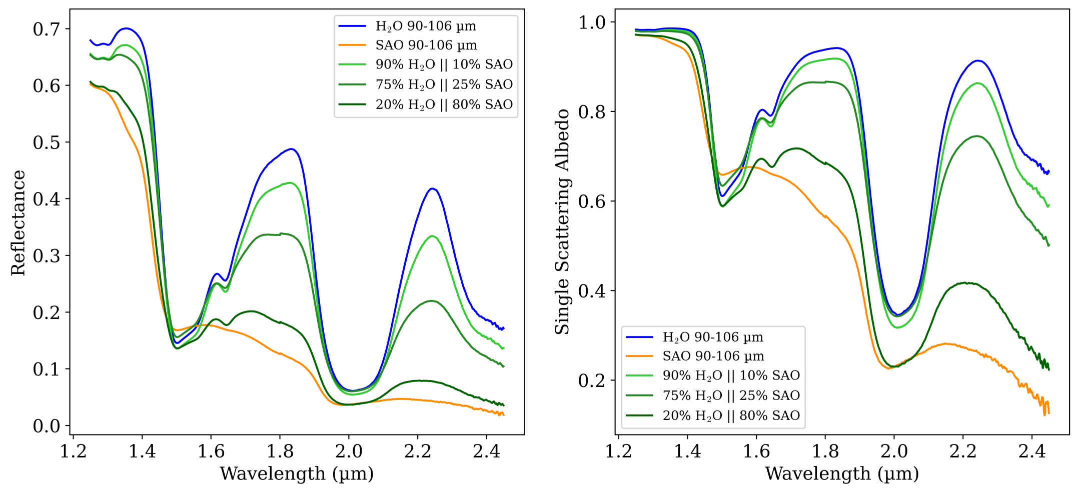


Figure 1: *Left panel:* Laboratory reflectance spectra of $H_2O$ ice, $H_2SO_4{\cdot}8H_2O$ (sulfuric acid octahydrate; SAO), and their mixtures at varying proportions (%wt) and grain sizes of 90–106 $\mu$m (Hayes and Li, 2025). The blue spectrum represents the $H_2O$ ice endmember, the orange spectrum represents the $H_2SO_4{\cdot}8H_2O$ endmember, and the spectra shown in shades of green correspond to mixtures of $H_2O$ ice and $H_2SO_4{\cdot}8H_2O$ at different ratios. All reflectance spectra were collected from Hayes and Li (2025). *Right panel:* Single scattering albedo spectra corresponding to the reflectance spectra, derived using radiative transfer theory based on the Hapke (1981) model (refer to *Section 2.2* for conversion details).

## 2. Observation and Methods

### *2.1. Laboratory spectra*

Reflectance spectra of $H_2O$ ice and $H_2SO_4{\cdot}8H_2O$ mixtures were measured at varying ratios and in the grain sizes of 90–106 $\mu$m (Hayes and Li, 2025). The measurements were conducted at ∼77 K under standard viewing geometry, with an incidence angle ($i$) of 30°, an emission angle ($e$) of 0°, and a phase angle ($g$) of 30° at the spectral wavelength of ∼1.25-2.45 $\mu$m. Although Europa's surface temperature is ∼120 K (e.g., Spencer et al., 1999; Carlson et al., 2009; Ashkenazy, 2019), reflectance spectra of $H_2O$ ice and $H_2SO_4{\cdot}8H_2O$ measured at 77 K can be used to represent Europa's surface relevant spectra, as spectral variations (absorption depths and position) over this temperature range are minor (e.g., Carlson et al., 2005; Mastrapa et al., 2008, 2009; Stephan et al., 2021; Hayes and Li, 2025). For details on the experimental setup and procedures, I refer readers to Hayes and Li (2025). The spectra of pure $H_2O$ ice and pure $H_2SO_4{\cdot}8H_2O$ obtained by Hayes and Li (2025) are used as endmembers for both the LM and RT spectral modeling. The mixture dataset includes three compositions: 90% $H_2O$ + 10% SAO, 75% $H_2O$ + 25% SAO, and 20% $H_2O$ + 80% SAO mixtures (by mass or %wt) at grain sizes of ∼100 (90–106) $\mu$m (Fig. 1). The $H_2SO_4{\cdot}8H_2O$ grains used in this study are spherical, whereas the $H_2O$ ice grains are angular to sub-angular (T. W. Hayes, 2025; personal communication).

*2.2. LM and RT modeling*

In linear mixture modeling, the mixture spectrum is represented as the weighted sum of the reflectances of each endmember, with the weights corresponding to their abundances (e.g., Emran et al., 2023):

$$r_m = \sum_{i=1}^{k} f_i \cdot r_i \ ; \ 0 \leq f_i \leq 1 \ ; \ \sum_{i=1}^{k} f_i = 1 \tag{1}$$

where $r_m$ is the reflectance of the mixture spectrum, $r_i$ is the reflectance of the $i^{th}$ constituent endmember, and $f_i$ is the fractional abundance (%wt) of the $i^{th}$ endmember (e.g., Dalton III et al., 2012; Emran et al., 2021; Emran and Stack, 2025). Using Eq. (1), I estimated the modeled abundances of $H_2O$ ice and $H_2SO_4{\cdot}8H_2O$ for reflectance spectra of mixtures.

In contrast, intimate mixture modeling based on radiative transfer accounts for the non-linear scattering properties of reflectance, but assumes linear behavior when reflectance is converted to single scattering albedo (Hapke, 1981, 2001, 2012; Mustard and Pieters, 1989; Mustard and Glotch, 2019). Therefore, I converted both the endmember and mixture reflectance spectra to single scattering albedo using the Hapke theory (Hapke, 1981) with the same viewing geometry and grain size as the measured reflectance spectra (Fig. 1). The reflectance (also known as radiance coefficient) in the Hapke model (Hapke, 1981) can be expressed as:

$$r(i, e, g) = \frac{w}{4} \cdot \frac{1}{\mu_e + \mu_i} \left\{ \left[1 + B(g)\right] P(g) + H(\mu_e) H(\mu_i) - 1 \right\} \tag{2}$$

where $r$ is the reflectance, $w$ is the average single-scattering albedo, $\mu_i$ and $\mu_e$ are the cosines of incidence angle ($i$) and emission angle ($e$), respectively, $B(g)$ is the backscattering function, $P(g)$ is the single-particle phase function, and $H(\mu_x)$ is the multiple scattering $H$ functions of Chandrasekhar (1960). Refer to relevant literature for details of these functions (e.g., Hapke, 1981, 2001, 2012). However, for the laboratory spectra considered in this study, I assume no backscattering ($B(g) = 0$) and an isotropic phase function ($P(g) = 1$), following Lapotre et al. (2017). Under these assumptions, the Hapke reflectance equation simplifies to (e.g., Mustard and Pieters, 1987, 1989):

$$r(i, e, g) \approx \frac{w}{4} \cdot \frac{1}{\mu_e + \mu_i} \cdot H(\mu_e) H(\mu_i) \tag{3}$$

The validity of Eq. 3 for abundance estimation has been tested against laboratory reflectance spectra of intimate mineral mixtures, under the assumption of isotropic scattering behavior of particulate media at phase angles of 15° – 40° (Mustard and Pieters, 1987, 1989). At these intermediate phase angles, the backscattering is assumed negligible ($B(g) << 1$) and becomes significant only at very small phase angles (< 10°; Mustard and Pieters 1987). Using this simplified method (Eq. 3), abundance estimates are accurate to within a few percent (%) when particle grain sizes are known (Mustard and Pieters, 1987, 1989).

The Chandrasekhar $H$ functions describing multiple scattering can be derived as (Hapke, 2002):

$$H(x) \approx \left[1 - wx\left(r_o + \frac{1-2r_o x}{2}\ln\left(\frac{1+x}{x}\right)\right)^{-1}\right] \tag{4}$$

$$r_o = \frac{1-\gamma}{1+\gamma} \tag{5}$$

$$\gamma = \sqrt{1-w} \tag{6}$$

where $r_o$ is the bihemispherical reflectance for isotropic scatterers, $\gamma$ is the albedo factor, and $x$ represents either the cosine of the incidence angle ($\mu_\mathrm{i} = \cos(i)$) or the emission angle ($\mu_\mathrm{e} = \cos(e)$).

The photon penetration depth ($\delta$) into a particulate surface or media is inversely proportional to the imaginary part ($k$) of the material's optical constant at a given wavelength (e.g., Born et al., 1999; Hapke, 2012). For both $H_2O$ ice and $H_2SO_4{\cdot}8H_2O$, the low $k$ values at NIR (e.g., Mastrapa et al., 2008, 2009; Carlson et al., 2005) result in $\delta$ on the order of hundreds of micrometers. Because the grain diameter ($d$ $\sim$100$\mu$m) is much smaller than the penetration depth ($d < \delta$), photons interact with multiple grains, making multiple scattering the dominant effect (e.g, Hapke, 1981, 2012). This process can induce significant spectral changes in intimate mixture even with trace amounts of material (e.g., Hayes and Li, 2025). Thus, multiple scattering terms ($H$-functions) were included in RT modeling (Eq. 3) to ensure accurate abundance estimates.

Upon conversion to single scattering albedo from the laboratory reflectance spectra using Eqs. (3)–(6), the RT spectral modeling can be expressed as follows (e.g., Stack and Milliken, 2015; Goudge et al., 2015; Lapotre et al., 2017):

$$w_m = \sum_{i=1}^{k} f_i \cdot w_i \tag{7}$$

where $w_m$ is the single scattering albedo of the mixture spectrum, $w_i$ is the single scattering albedo of the $i^{th}$ constituent endmember, and $f_i$ is the relative fractional (geometric) cross section of the $i^{th}$ endmember. The relative geometric cross-section (also known as F-parameter) is a function of the mass fraction, density, and particle diameter of components in a mixture (e.g., Mustard and Pieters, 1987, 1989).

While grain size has a major influence on the spectral characteristics of materials, grain shape can also affect the resulting spectra (e.g., Shkuratov and Grynko, 2005; Hapke, 2012). However, since both endmembers— $H_2O$ ice and $H_2SO_4{\cdot}8H_2O$ —were modeled with the same grain size ($\sim$100$\mu$m), shape effects were ignored. Under simplified assumptions, such as similar grain sizes and densities of particles, $f_i$ can be considered equivalent to the fractional contribution or abundance (%wt) of the corresponding endmember (e.g., Mustard and Pieters, 1987). However, the densities of $H_2O$ ice and SAO differ slightly under outer Solar System–relevant temperatures— $H_2O$ ice has a density of $\sim$1 g/cm$^3$ (e.g., Blackman and Lisgarten, 1957; Yarnall and Hudson, 2022), whereas the slightly denser $H_2SO_4{\cdot}8H_2O$ has a density of $\sim$1.3 g/cm$^3$ (Maynard-Casely et al., 2012, 2013). Accordingly, the relative fractional cross-section for $H_2O$ ice and $H_2SO_4{\cdot}8H_2O$ was scaled by their respective density factors in Eq. (7), and the fractional abundances in the mixtures were adjusted accordingly.

In this study, I employed the Markov Chain Monte Carlo (MCMC) simulation technique (Hogg and Foreman-Mackey, 2018) to estimate the model abundances using Equations (1) and 7), following the approach outlined in Emran et al. (2021). The MCMC technique used here adopts a Bayesian inference framework to predict the model parameters, e.g., the abundances of each endmember. Using the *emcee* Python package (Foreman-Mackey et al., 2013), I implemented the models and performed 1,000 iterations to estimate the parameters.

## 3. Results

Fig. 2 presents the modeled spectra generated using the linear mixture (left panel) and radiative transfer (right panel) modeling approaches, along with the estimated best-fit mean abundances (Est.) for $H_2O$ ice and $H_2SO_4{\cdot}8H_2O$ across different laboratory mixtures. The estimated abundances vary with mixture ratios (%wt), as shown in the row-wise subplots (Fig. 2).

For the 90% $H_2O$ ∥ 10% SAO mixture (top row in Fig. 2), the RT modeling results in better abundance estimates of $H_2O$ ice and $H_2SO_4{\cdot}8H_2O$ than the LM modeling, even though the LM modeling produces a lower root mean square error (RMSE) value— 0.008 (LM) vs 0.011 (RT). Specifically, the LM and RT estimated mean $\pm$ 1$\sigma$ abundances are 82±4% $H_2O$ ∥ 18±4% SAO and 89±3% $H_2O$ ∥ 11±3% SAO, respectively (Table 1). Thus, the mean abundance offset from the true composition is ±8% for LM and ±1% for RT modeling (Fig. 3).

In the case of the 75% $H_2O$ ∥ 25% SAO mixture (middle row in Fig. 2), the abundance estimates by the RT modeling again outperform the LM modeling results. Moreover, the RT modeling also shows a lower RMSE value than the LM modeling— 0.011 vs 0.018, respectively. The estimated abundances are 60±4% $H_2O$ ∥ 40±4% SAO for LM and 72±4% $H_2O$ ∥ 28±4% SAO for RT modeling (Table 1), resulting in mean abundance offsets of ±15% (LM) and ±3% (RT) from the true values (Fig. 3).

Lastly, for the 20% $H_2O$ ∥ 80% SAO mixture (bottom row in Fig. 2), both models perform comparably in terms of RMSE value (0.012 by RT and 0.011 by LM), though the RT modeling still results in closer abundance estimates to the true abundance. The LM and RT estimates are 14±4%$H_2O$ ∥ 86±4% SAO and 18±5% $H_2O$ ∥ 82±5% SAO, respectively (Table 1), corresponding to mean abundance offsets of ±6% and ±2%, respectively (Fig. 3).

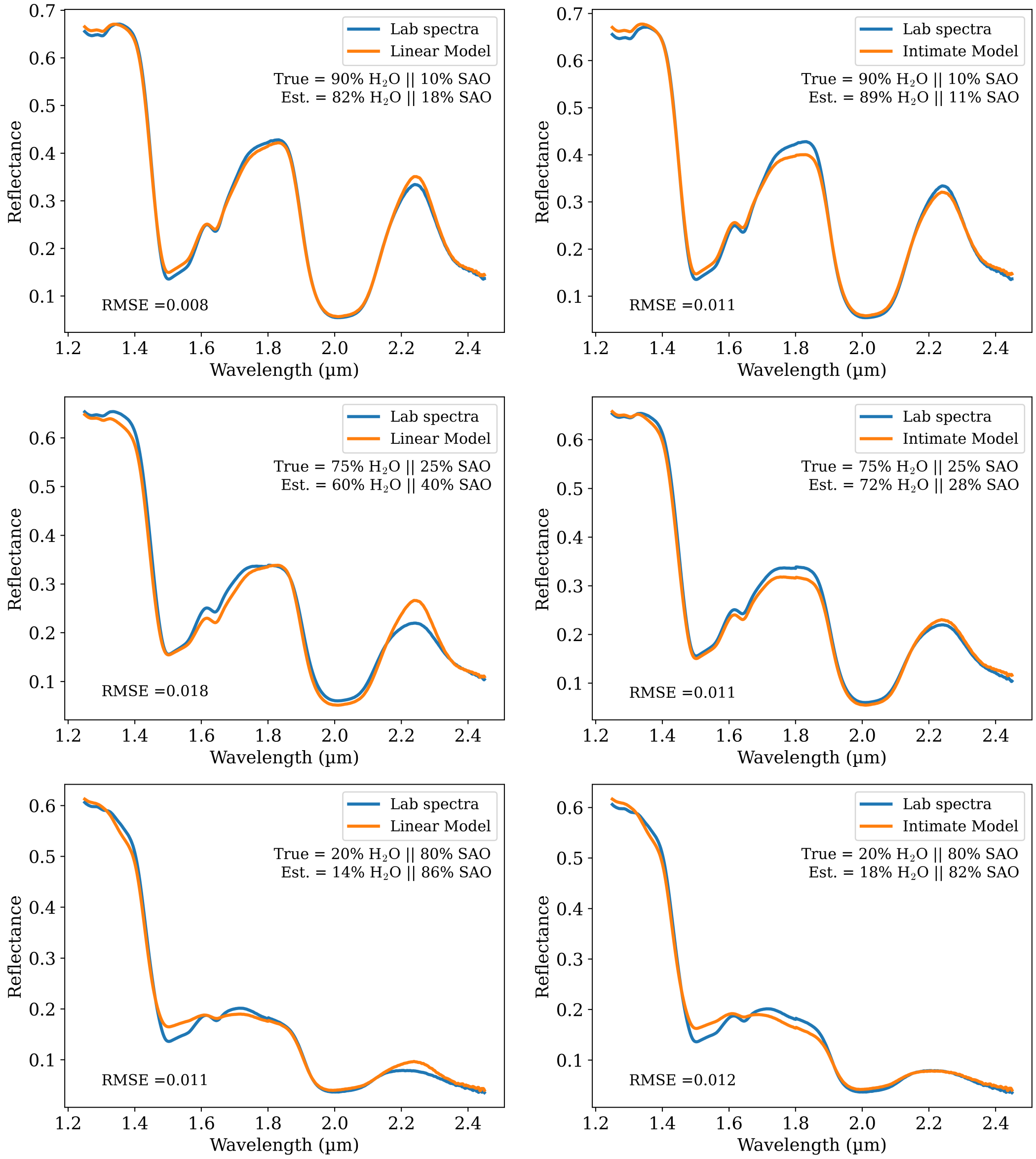


Figure 2: Comparison of linear mixture modeling (left panel) and intimate mixture modeling using the Hapke (1981) radiative transfer theory (right panel). In each subplot, the blue spectrum represents the laboratory reflectance spectrum of the $H_2O$–SAO mixture (Hayes and Li, 2025), while the orange spectrum shows the modeled spectrum from either the LM or Hapke-based RT modeling. The true (laboratory) and estimated (model-derived) mean abundances of $H_2O$ ice and sulfuric acid octahydrate (SAO) are indicated in each subplot, along with the root mean square error (RMSE) of the spectral fit.

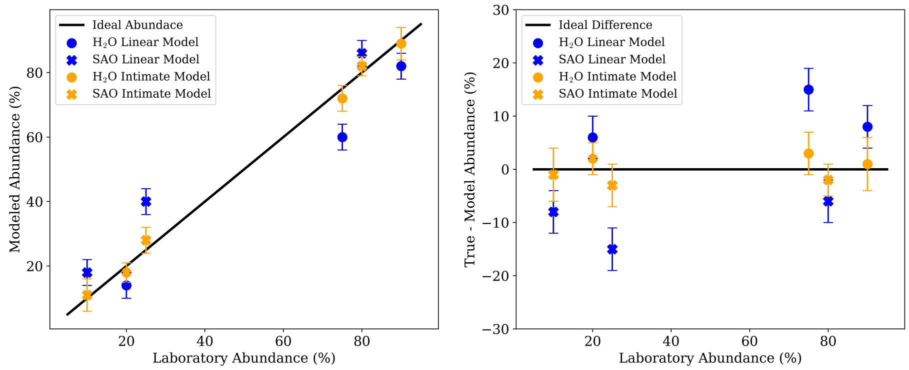


Figure 3: Comparison of modeled abundances (mean $\pm$ $1\sigma$) of $H_2O$ ice and sulfuric acid octahydrate (SAO) using the linear mixture modeling and the intimate mixture modeling based on the Hapke (1981) radiative transfer theory. *Left panel*: Modeled abundances plotted against the expected (ideal) laboratory abundances. Blue and orange markers represent estimates from the LM and Hapke-based RT modeling, respectively. Circle and cross markers represent $H_2O$ ice and SAO abundances, respectively, by the corresponding mixture modeling. *Right panel*: Difference between the laboratory (true) abundances and the modeled abundances (True-Model abundance) for each component using both modeling approaches (LM and RT).

Table 1: Modeled abundances of $H_2O$ ice and sulfuric acid octahydrate (SAO) using linear mixture modeling and intimate mixture modeling based on the Hapke (1981) radiative transfer theory. Abundances are reported as fractional percentages (%wt) as mean $\pm$ $1\sigma$.

| **Mixture abundance (laboratory mixture)** | **Linear mixture (LM) abundance** | | **Intimate mixture (RT) abundance** | |
|---|---|---|---|---|
| | $H_2O$ (%) | SAO (%) | $H_2O$ (%) | SAO (%) |
| 90% $H_2O$ + 10% SAO | 82 $\pm$ 4 | 18 $\pm$ 4 | 89 $\pm$ 3 | 11 $\pm$ 3 |
| 75% $H_2O$ + 25% SAO | 60 $\pm$ 4 | 40 $\pm$ 4 | 72 $\pm$ 4 | 28 $\pm$ 4 |
| 20% $H_2O$ + 80% SAO | 14 $\pm$ 4 | 86 $\pm$ 4 | 18 $\pm$ 5 | 82 $\pm$ 5 |

## 4. Discussion and implications for Europa

In this study, I compared two widely-used spectral modeling approaches— linear mixture modeling and radiative transfer–based intimate mixture modeling —against laboratory spectra of $H_2O$ ice and $H_2SO_4{\cdot}8H_2O$ mixtures at varying ratios (%wt) relevant to Europa (Hayes and Li, 2025). The results suggest several key insights regarding the future implementation of spectral modeling (LM and RT) for constraining surface compositional abundances, and by extension, for interpreting the geological processes and surface compositional evolution on Jupiter's moon.

This study demonstrates that the spectral fit quality—quantified by metrics such as root mean square error (RMSE) or chi-square ($\chi^2$) values—does not necessarily reflect the accuracy of the estimated compositional abundances. For example, in the 90% $H_2O$ ∥ 10% SAO mixture case, the LM model resulted in a lower RMSE compared to the RT model (also, the LM visually shows a closer spectral fit to the laboratory spectra), yet the RT approach produced significantly more accurate abundance estimates. Conversely, in another case (75% $H_2O$ ∥ 25% SAO mixture), a better spectral fit—as indicated by a lower RMSE—did correspond to abundance estimates that closely matched the true compositional abundance. This suggests that while a lower RMSE or $\chi^2$ value may sometimes reflect improved abundance accuracy, it is not a consistent indicator or does not guarantee the model's performance in compositional retrieval (abundance estimates of surface materials) on Europa.

Across all tested mixture ratios, the RT modeling consistently produces mean abundance estimates that are within ±5% of the true laboratory values for $H_2O$ ice and SAO mixtures with ∼100 $\mu$m grains. In contrast, the LM modeling tends to result in larger deviations, typically in the range of ±5–15%. This observation may suggest that Europa's surface is more accurately represented by an intimate mixture (RT) modeling, regardless of geologic units (e.g., Greeley et al., 2000; Prockter and Patterson, 2009; Daubar et al., 2024; Leonard et al., 2024) across the leading and trailing hemispheres, given that the grain sizes are comparable (∼100 $\mu$m). However, the deviation in the LM estimates is relatively smaller when sulfuric acid abundance dominates in the mixture. For instance, the LM estimated abundances deviate by only ±6% from the true values in a high-SAO scenario (80% in mixture). A similar deviation in abundance (±8%) is also observed where sulfuric acid is present in trace amounts, such as in ∼10% of the mixture. Thus, in regions where surface materials show a patchy distribution and the abundance of sulfuric acid is either very high (> 80%) or very low (∼10%), the LM model produces viable abundance estimates with ∼100 $\mu$m grains. For instance, a surface composed of patches of dark and bright materials on Europa (Fig. 4)— arranged in a checkerboard-like distribution— may favor the application of the LM model (e.g., Shirley et al., 2016), as this approach is based on areal mixing of materials. In contrast, RT modeling is better suited for regions where surface materials are thoroughly mixed at the particle level—similar to a lunar regolith–type intimately mixed surface (e.g., Shkuratov et al., 1999)—rather than being segregated into distinct patches, which could result from thermal segregation of surface materials (Spencer, 1987; Sorli and Hayne, 2023). RT modeling may particularly be relevant in areas influenced by radiolytic processes on Europa (Fig. 4; Shirley et al., 2016), where radiation likely interacted uniformly with the molecules in the surface regolith of the moon (Carlson et al., 1999a, 2002). Nonetheless, regardless of the magnitude of deviation, both LM and RT modeling consistently overestimates the abundance of $H_2SO_4{\cdot}8H_2O$ and underestimating $H_2O$ ice (Table 1). These discrepancies are consistently observed across all laboratory mixture cases analyzed in this study (see Fig. 3).

Photons at NIR wavelengths penetrate a finite depth into a particulate surface (e.g., Born et al., 1999). This penetration depth is a critical factor, as it governs multiple scattering effects in intimate mixtures or granular media (Hapke, 1981, 2012). The areal mixing approach assumes that the surface is composed of patches with uniform composition and does not account for variations in depth within grains or regolith. Under this assumption, each photon interacts with only a single endmember, thereby neglecting multiple scattering between different compositional units or grains. In contrast, intimate mixtures exhibit highly nonlinear spectral behavior at NIR wavelengths be-

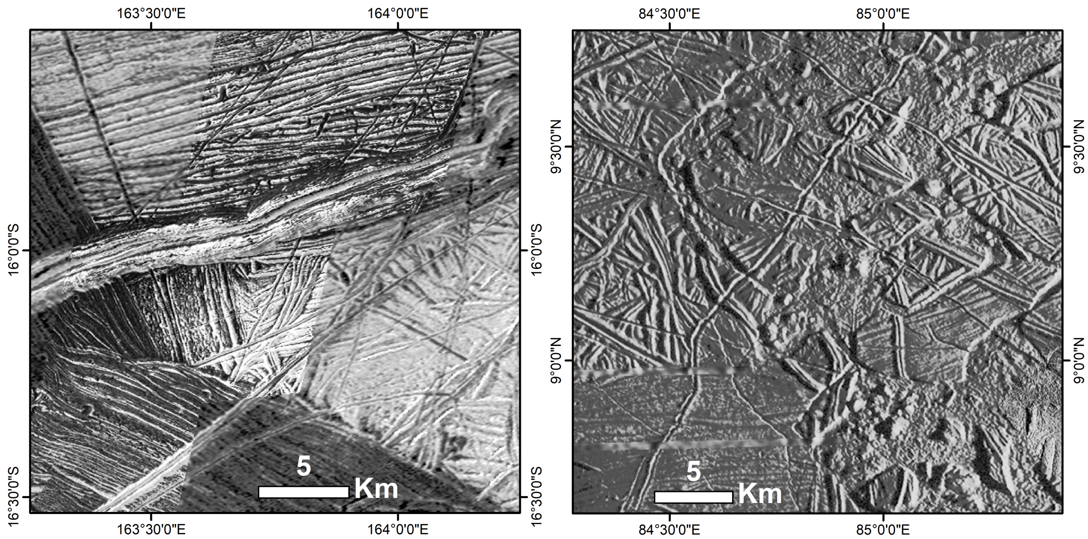


Figure 4: *Left panel:* Patches of dark and bright materials on Europa observed in a high-resolution image from the Galileo Solid State Imaging (SSI) system (Belton et al., 1992). The image is centered at approximately 16°S, 163°45'E, with a spatial resolution of ∼50 m/pixel. *Right panel:* A high-resolution Galileo/SSI image of Europa's chaos terrains on the trailing hemisphere (near center)—an area exposed to radiolytic processes (e.g., Carlson et al., 1999a, 2002)— showing no discernible dark and bright patches. The image is centered at approximately 9°15'N, 84°50'E, with a spatial resolution of ∼50 m/pixel. Both SSI images are adopted from Malaska et al. (2024).

cause light is multiply scattered among mineral species or grains (Hapke, 1981, 2012; Mustard and Pieters, 1987, 1989). As a result, even trace amounts of material can significantly influence the observed spectra of an intimate mixture (e.g., Hapke, 2012; Hayes and Li, 2025). These limitations of the LM modeling approach— which ignores photon penetration depth, multiple scattering, and compositional variation with depth— likely contribute to the higher discrepancies in abundance estimates of mixture components, particularly when grain sizes are much smaller than the photon penetration depth. By comparison, RT modeling accounts for photon penetration depth by incorporating multiple scattering effects when estimating the complex spectral properties of mixtures. While multiple scattering strongly influences reflectance spectra used in LM modeling, its effects are reduced when reflectance is converted to single scattering albedo (e.g., Hapke, 1981, 2012). In this form, the single scattering albedo spectra of a mixture is approximately linearly proportional to the relative fractional abundances of the constituent materials (e.g., Hapke, 1981, 2012; Mustard and Glotch, 2019). Thus, by properly accounting for the complexity of light scattering in granular or particulate media, RT modeling provides more accurate abundance estimates—within ±5% in this study— compared to LM modeling.

The performance of the LM and RT modeling was compared here using laboratory spectra of $H_2O$ ice and sulfuric acid with grain sizes ranging from 90–106 $\mu$m (Hayes and Li, 2025). Due to the limited availability of laboratory spectra for other grain sizes for

$H_2O$ and $H_2SO_4{\cdot}8H_2O$ mixtures, the influence of grain size on the modeling performance for these mixtures could not be directly assessed. However, the effect of grain size on reflectance spectra—and thus on spectral modeling—cannot be overlooked, as it is well-established that grain size significantly affects spectral features (e.g., Stephan et al., 2021; Mastrapa et al., 2008; Emran and Chevrier, 2023). Relatively small grain sizes—ranging from 20–30 $\mu$m on the leading hemisphere to $\sim$100 $\mu$m near the poles of the trailing hemisphere—have been suggested to characterize Europa's surface (e.g., Kieffer and Smythe, 1974; Hansen and McCord, 2004; Carlson et al., 2005, 2009; Moore et al., 2009; Becker et al., 2024). However, spectral analyses suggest the presence of coarser grains—up to $\sim$1 mm in size—particularly in regions such as large lineae, microchaos, and band geologic units (Ligier et al., 2016; Emran, 2025a). Thus, the findings presented here are most applicable to regions on Europa where grain sizes are relatively small, around $\sim$100 $\mu$m. In contrast, terrains associated with effusive cryovolcanism (viz. surface flow) or surface–subsurface exchange, such as microchaos, are suggested to host coarser grains, potentially up to $\sim$1 mm in size (Ligier et al., 2016; Emran, 2025a). Consequently, I acknowledge that the results of this study have not been validated for those regions with coarser surface materials. A separate investigation using laboratory spectra with a broader range of grain sizes—including mixtures containing both micron- and millimeter-scale diameter grains—is warranted to assess the impact of grain size on spectral modeling accuracy. Notably, a detailed study comparing the accuracy of LM and RT modeling for $H_2O$ ice mixtures with coarse ($\sim$1 mm) and fine ($\sim$100 $\mu$m) grains relevant to Europa is presented in Emran (2025b).

Moreover, this study investigated the accuracy of LM and RT modeling using the reflectance spectra of the binary mixtures of $H_2O$ ice and SAO— the two major components identified on Europa (e.g., Moroz, 1966; Pilcher et al., 1972; Carlson et al., 1999a, 2005, 2009; Becker et al., 2024)— at different mixing ratios (Hayes and Li, 2025). However, Europa's surface is also hypothesized to host other species, such as $CO_2$ (Villanueva et al., 2023), $H_2O_2$ (Carlson et al., 1999b), $SO_2$ (Lane et al., 1981), $NH_3$-bearing compounds (Emran, 2025a), and various hydrated sulfate and chlorine (Cl-bearing) salts (e.g., Davis and Brown 2024; Becker et al. 2024, and references therein). To comprehensively assess the performance of LM and RT modeling, it is important to validate these approaches against mixtures that include a broader suite of materials. While laboratory spectra of these species would be invaluable for such testing, well-constrained reflectance spectra of intimate mixtures are limited and currently available for binary mixtures of $H_2O$ ice and $H_2SO_4{\cdot}8H_2O$. Thus, I emphasize the need for a robust set of optical constants and laboratory mixture spectra for these additional constituents, as they are essential for a complete understanding of Europa's surface composition as constrained through spectral modeling using either areal mixing or radiative transfer approaches.

The use of zero backscattering and isotropic scattering in this study was based on the controlled viewing geometry (phase angle of 30°) of the laboratory spectra and the known grain sizes of the materials. For remotely sensed data, such as from telescopes or spacecraft, however, the scenario differs— viewing geometry varies from observation to observation, and the grain sizes of the regolith are often poorly constrained or unknown. In such cases, photometric analyses of planetary surfaces are performed using the Hapke radiative transfer model (Hapke, 1981) to estimate surface backscattering and phase parameters, as done for Europa (e.g., Buratti and Veverka, 1985; Buratti, 1995; Domingue and Hapke, 1992; Belgacem et al., 2018, 2020). Accurate backscattering and phase parameters are therefore essential for constraining reliable abundance estimates of surface compositions using RT modeling from ground- and space-based observations.

Nonetheless, both LM and RT models produce acceptable results— within ±10% uncertainty— under specific compositional conditions ($H_2O$ and $H_2SO_4{\cdot}8H_2O$ mixtures with grain sizes around $\sim$100 $\mu$m) relevant to regions on Europa. This includes the regions where $H_2SO_4{\cdot}8H_2O$ is the dominant component ($>$ 80% abundance), such as the trailing hemisphere (e.g., Carlson et al., 2005), as well as regions where $H_2SO_4{\cdot}8H_2O$ occurs in trace amounts ($\sim$10% abundance), as observed in some parts of the leading hemisphere (Dalton III et al., 2013; Ligier et al., 2016). Overall, the results support the use of radiative transfer-based intimate mixture spectral modeling (e.g., Hapke, 1981; Shkuratov et al., 1999) as the preferred method for constraining the surface composition of Europa. However, linear mixture modeling remains a viable approach in compositional regimes where the abundance of sulfuric acid is either very high or very low, allowing for flexibility depending on the available data and modeling constraints. These findings provide a valuable guideline for future compositional analyses using imaging spectrometers, such as ESA-JUICE's Moons and Jupiter Imaging Spectrometer (MAJIS; Poulet et al., 2024) and NASA-Europa Clipper's Mapping Imaging Spectrometer for Europa (MISE; Blaney et al., 2024), for an improved understanding of the composition of Europa's surface.

### Notations

$r$ = Reflectance or radiance factor
$r_m$ = Reflectance of mixture
$r_o$ = Bihemispherical reflectance for isotropic scatterers
$f$ = Fractional abundance/ factor
$w$ = Single scattering albedo (SSA)
$w_m$ = SSA of the mixture spectrum
$i$ = Incidence angle
$e$ = Emission angle
$g$ = Phase angle
$B(g)$ = Backscattering function
$P(g)$ = Single-particle phase function
$H(x)$ = Chandrasekhar's H functions
$\mu_\mathrm{i}$ = Cosine of the incidence angle
$\mu_\mathrm{e}$ = Cosine of the emission angle
$\gamma$ = Albedo factor
$\delta$ = Photon penetration depth
$k$ = Imaginary part of optical constants
$d$ = Diameter or Grain Size

### Data Availability

The laboratory spectral data used in this study were collected from Hayes and Li (2025) and can be accessed at https://doi.org/10.5281/zenodo.13852483. Galileo Solid State Imaging (SSI) data used in this study can be found in the National Aeronautics and Space Administration's Planetary Data System: Imaging Node Server at https://pdsimage2.wr.usgs.gov/ (Malaska et al., 2024).

### Declaration of generative AI

During the preparation of this work the author(s) used OpenAI in order to improve the readability and language of the manuscript. After using this tool/service, the author(s) reviewed and edited the content as needed and take(s) full responsibility for the content of the publication.

### Acknowledgments

This research was carried out at the Jet Propulsion Laboratory (JPL), California Institute of Technology, under a contract with the National Aeronautics and Space Administration (80NM0018D0004). I acknowledge JPL's High-Performance Computing supercomputer facility, which was funded by JPL's Information and Technology Solutions Directorate. I also thank Kathryn M. Stack for valuable discussions on spectral modeling. 

## References


Ashkenazy, Y., 2019. The surface temperature of europa. Heliyon 5.

Becker, T., Zolotov, M.Y., Gudipati, M., Soderblom, J., McGrath, M., Henderson, B., Hedman, M., Choukroun, M., Clark, R., Chivers, C., et al., 2024. Exploring the composition of europa with the upcoming europa clipper mission. Space Science Reviews 220, 49.

Belgacem, I., Schmidt, F., Jonniaux, G., 2018. Estimation of hapke's parameters on selected areas of europa using a bayesian approach, in: Lunar and Planetary Science Conference (LPSC), p. Abstract #1051.

Belgacem, I., Schmidt, F., Jonniaux, G., 2020. Regional study of europa's photometry. Icarus 338, 113525.

Belton, M.J., Klaasen, K.P., Clary, M.C., Anderson, J.L., Anger, C.D., Carr, M.H., Chapman, C.R., Davies, M.E., Greeley, R., Anderson, D., et al., 1992. The galileo solid-state imaging experiment. Space Science Reviews 60, 413–455.

Blackman, M., Lisgarten, N., 1957. The cubic and other structural forms of ice at low temperature and pressure. Proceedings of the Royal Society of London. Series A. Mathematical and Physical Sciences 239, 93–107.

Blaney, D.L., Hibbitts, K., Diniega, S., Davies, A.G., Clark, R.N., Green, R.O., Hedman, M., Langevin, Y., Lunine, J., McCord, T.B., et al., 2024. The mapping imaging spectrometer for europa (mise). Space Science Reviews 220, 80.

Born, M., Wolf, E., Bhatia, A.B., et al., 1999. Principles of optics: electromagnetic theory of propagation, interference and diffraction of light. (No Title) .

Brown, M., Hand, K., 2013. Salts and radiation products on the surface of europa. The Astronomical Journal 145, 110.

Buratti, B., 1995. Photometry and surface structure of the icy galilean satellites. Journal of Geophysical Research 100, 19061–19066.

Buratti, B., Veverka, J., 1985. Photometry of rough planetary surfaces: The role of multiple scattering. Icarus 64, 320–328.

Carlson, R., Anderson, M., Johnson, R., Schulman, M., Yavrouian, A., 2002. Sulfuric acid production on europa: the radiolysis of sulfur in water ice. Icarus 157, 456–463.

Carlson, R., Anderson, M., Johnson, R., Smythe, W., Hendrix, A., Barth, C., Soderblom, L., Hansen, G., McCord, T., Dalton, J., et al., 1999b. Hydrogen peroxide on the surface of europa. Science 283, 2062–2064.

Carlson, R., Anderson, M., Mehlman, R., Johnson, R., 2005. Distribution of hydrate on europa: Further evidence for sulfuric acid hydrate. Icarus 177, 461–471.

Carlson, R., Calvin, W., Dalton, J., Hansen, G., Hudson, R., Johnson, R., McCord, T., Moore, M., 2009. Europa's surface composition. Europa 283.

Carlson, R., Johnson, R., Anderson, M., 1999a. Sulfuric acid on europa and the radiolytic sulfur cycle. Science 286, 97–99.

Carlson, R.W., Weissman, P., Smythe, W.D., Mahoney, J., Science, N., Teams, E., 1992. Near-infrared mapping spectrometer experiment on galileo. Space Science Reviews 60, 457–502.

Chandrasekhar, S., 1960. Radiative transfer. Dover Publications, Mineola, New York.

Dalton III, J., Cassidy, T., Paranicas, C., Shirley, J., Prockter, L., Kamp, L., 2013. Exogenic controls on sulfuric acid hydrate production at the surface of europa. Planetary and Space Science 77, 45–63.

Dalton III, J., Shirley, J., Kamp, L., 2012. Europa's icy bright plains and dark linea: Exogenic and endogenic contributions to composition and surface properties. Journal of Geophysical Research: Planets 117.

Dalton III, J.B., 2007. Linear mixture modeling of europa's non-ice material based on cryogenic laboratory spectroscopy. Geophysical research letters 34.

Daubar, I.J., Hayes, A.G., Collins, G., Craft, K.L., Rathbun, J., Spencer, J.R., Wyrick, D.Y., Bland, M.T., Davies, A.G., Ernst, C.M., et al., 2024. Planned geological investigations of the europa clipper mission. Space Science Reviews 220, 18.

Davis, M.R., Brown, M.E., 2024. Pwyll and manannán craters as a laboratory for constraining irradiation timescales on europa. The Planetary Science Journal 5, 107.

Domingue, D., Hapke, B., 1992. Disk-resolved photometric analysis of european terrains. Icarus 99, 70–81.

Emran, A., 2025a. Detection of an nh3 absorption band at 2.2um on europa. The Planetary Science Journal [accepted].

Emran, A., 2025b. Spectral mixture modeling with laboratory near-infrared data ii: Effects of grain size and implication for europa. Icarus [under review], X.

Emran, A., Chevrier, V., 2022. Uncertainty in grain size estimations of volatiles on trans-neptunian objects and kuiper belt objects. The Astronomical Journal 163, 196.

Emran, A., Chevrier, V., 2023. Discrepancy in grain size estimation of h2o ice in the outer solar system. Research in Astronomy and Astrophysics 23, 035015.

Emran, A., Dalle Ore, C., Cruikshank, D., Cook, J., 2023. Surface composition of pluto's kiladze area and relationship to cryovolcanism. Icarus 404, 115653.

Emran, A., Marzen, L., King Jr, D., Chevrier, V., 2021. Thermophysical and compositional analyses of dunes at hargraves crater, mars. The Planetary Science Journal 2, 218.

Emran, A., Stack, K., 2025. Understanding compositional evolution of hollows at dominici crater, mercury. Icarus 435, 116576.

Foreman-Mackey, D., Hogg, D.W., Lang, D., Goodman, J., 2013. emcee: the mcmc hammer. Publications of the Astronomical Society of the Pacific 125, 306.

Goudge, T.A., Mustard, J.F., Head, J.W., Salvatore, M.R., Wiseman, S.M., 2015. Integrating crism and tes hyperspectral data to characterize a halloysite-bearing deposit in kashira crater, mars. Icarus 250, 165–187.

Greeley, R., Figueredo, P.H., Williams, D.A., Chuang, F.C., Klemaszewski, J.E., Kadel, S.D., Prockter, L.M., Pappalardo, R.T., Head III, J.W., Collins, G.C., et al., 2000. Geologic mapping of europa. Journal of Geophysical Research: Planets 105, 22559–22578.

Hansen, G.B., McCord, T.B., 2004. Amorphous and crystalline ice on the galilean satellites: A balance between thermal and radiolytic processes. Journal of Geophysical Research: Planets 109.

Hapke, B., 1981. Bidirectional reflectance spectroscopy: 1. theory. Journal of Geophysical Research: Solid Earth 86, 3039–3054.

Hapke, B., 2001. Space weathering from mercury to the asteroid belt. Journal of Geophysical Research: Planets 106, 10039–10073.

Hapke, B., 2002. Bidirectional reflectance spectroscopy: 5. the coherent backscatter opposition effect and anisotropic scattering. Icarus 157, 523–534.

Hapke, B., 2012. Theory of reflectance and emittance spectroscopy. Cambridge university press.

Hayes, T., Li, S., 2025. Insights for hydrated sulfuric acid on europa's surface from a combined orbital–experimental approach. Icarus 434, 116543.

Hogg, D.W., Foreman-Mackey, D., 2018. Data analysis recipes: Using markov chain monte carlo. The Astrophysical Journal Supplement Series 236, 11.

Keshava, N., Mustard, J.F., 2002. Spectral unmixing. IEEE signal processing magazine 19, 44–57.

Khuller, A.R., Emran, A., 2025. Quantitative evaluation of the delta-eddington, hapke, and shkuratov models for predicting the albedo and inferring the grain radius of ice. Icarus , 116671.

Kieffer, H.H., Smythe, W., 1974. Frost spectra: Comparison with jupiter's satellites. Icarus 21, 506–512.

Lane, A., Nelson, R., Matson, D., 1981. Evidence for sulphur implantation in europa's 511 uv absorption band. Nature 292, 38–39.

Lapotre, M.G., Ehlmann, B.L., Minson, S.E., 2017. A probabilistic approach to remote compositional analysis of planetary surfaces. Journal of Geophysical Research: Planets 122, 983–1009.

Leonard, E.J., Patthoff, D.A., Senske, D.A., 2024. Global geologic map of Europa. Technical Report. US Geological Survey.

Li, S., Li, L., 2011. Radiative transfer modeling for quantifying lunar surface minerals, particle size, and submicroscopic metallic fe. Journal of Geophysical Research: Planets 116.

Li, S., Milliken, R.E., 2015. Estimating the modal mineralogy of eucrite and diogenite meteorites using visible–near infrared reflectance spectroscopy. Meteoritics & Planetary Science 50, 1821–1850.

Ligier, N., Poulet, F., Carter, J., Brunetto, R., Gourgeot, F., 2016. Vlt/sinfoni observations of europa: New insights into the surface composition. The Astronomical Journal 151, 163.

Liu, Y., Glotch, T.D., Scudder, N.A., Kraner, M.L., Condus, T., Arvidson, R.E., Guinness, E.A., Wolff, M.J., Smith, M.D., 2016. End-member identification and spectral mixture analysis of crism hyperspectral data: A case study on southwest melas chasma, mars. Journal of Geophysical Research: Planets 121, 2004–2036.

Malaska, M., Valenti, M., Davies, A., Shirley, J., Phillips, C., Fraeman, A., Galbert, V., Lopes, R., Prockter, L., Cahill, J., et al., 2024. Updated and registered europa nims hyperspectral map products. NASA Planetary Data System , 130.

Mastrapa, R., Bernstein, M., Sandford, S., Roush, T., Cruikshank, D., Dalle Ore, C., 2008. Optical constants of amorphous and crystalline h2o-ice in the near infrared from 1.1 to 2.6 $\mu$m. Icarus 197, 307–320.

Mastrapa, R., Sandford, S., Roush, T., Cruikshank, D., Dalle Ore, C., 2009. Optical constants of amorphous and crystalline h2o-ice: 2.5–22 $\mu$m (4000–455 cm- 1) optical constants of h2o-ice. The Astrophysical Journal 701, 1347.

Maynard-Casely, H., Wallwork, K., Avdeev, M., 2013. A new material for the icy galilean moons: The structure of sulfuric acid hexahydrate. Journal of Geophysical Research: Planets 118, 1895–1902.

Maynard-Casely, H.E., Brand, H.E., Wallwork, K.S., 2012. Structure and thermal expansion of sulfuric acid octahydrate. Applied Crystallography 45, 1198–1207.

Mermy, G.C., Schmidt, F., Andrieu, F., Cornet, T., Belgacem, I., Altobelli, N., 2023. Selection of chemical species for europa's surface using galileo/nims. Icarus 394, 115379.

Mishra, I., Lewis, N., Lunine, J., Hand, K.P., Helfenstein, P., Carlson, R., MacDonald, R.J., 2021. A comprehensive revisit of select galileo/nims observations of europa. The Planetary Science Journal 2, 183.

Moore, J.M., Black, G., Buratti, B., Phillips, C.B., Spencer, J., Sullivan, R., 2009. Surface properties, regolith, and landscape degradation, in: Europa. University of Arizona Press Tucson, pp. 329–349.

Moroz, V., 1966. The spectra of jupiter and saturn in the 1.0–2.5 $\mu$m region. Soviet Astronomy 10, 457.

Mustard, J.F., Glotch, T.D., 2019. Theory of reflectance and emittance spectroscopy of geologic materials in the visible and infrared regions. Remote compositional analysis: Techniques for understanding spectroscopy, mineralogy, and geochemistry of planetary surfaces , 21–41.

Mustard, J.F., Pieters, C.M., 1987. Quantitative abundance estimates from bidirectional reflectance measurements. Journal of Geophysical Research: Solid Earth 92, E617–E626.

Mustard, J.F., Pieters, C.M., 1989. Photometric phase functions of common geologic minerals and applications to quantitative analysis of mineral mixture reflectance spectra. Journal of Geophysical Research: Solid Earth 94, 13619–13634.

Pilcher, C., Ridgway, S., McCord, T., 1972. Galilean satellites: Identification of water frost. Science 178, 1087–1089.

Poulet, F., Erard, S., 2004. Nonlinear spectral mixing: Quantitative analysis of laboratory mineral mixtures. Journal of Geophysical Research: Planets 109.

Poulet, F., Piccioni, G., Langevin, Y., Dumesnil, C., Tommasi, L., Carlier, V., Filacchione, G., Amoroso, M., Arondel, A., D'Aversa, E., et al., 2024. Moons and jupiter imaging spectrometer (majis) on jupiter icy moons explorer (juice). Space Science Reviews 220, 27.

Prockter, L.M., Patterson, G.W., 2009. Morphology and evolution of europa's ridges and bands. Europa , 237–258.

Shirley, J.H., Dalton III, J.B., Prockter, L.M., Kamp, L.W., 2010. Europa's ridged plains and smooth low albedo plains: Distinctive compositions and compositional gradients at the leading side–trailing side boundary. Icarus 210, 358–384.

Shirley, J.H., Jamieson, C.S., Dalton III, J.B., 2016. Europa's surface composition from near-infrared observations: A comparison of results from linear mixture modeling and radiative transfer modeling. Earth and Space Science 3, 326–344.

Shkuratov, Y., Starukhina, L., Hoffmann, H., Arnold, G., 1999. A model of spectral albedo of particulate surfaces: Implications for optical properties of the moon. Icarus 137, 235–246.

Shkuratov, Y.G., Grynko, Y.S., 2005. Light scattering by media composed of semitransparent particles of different shapes in ray optics approximation: consequences for spectroscopy, photometry, and polarimetry of planetary regoliths. Icarus 173, 16–28.

Sorli, K., Hayne, P., 2023. Thermal segregation as a mechanism for darkening ridge troughs on europa, in: AAS/Division for Planetary Sciences Meeting Abstracts# 55, pp. 210–03.

Spencer, J.R., 1987. Thermal segregation of water ice on the galilean satellites. Icarus 69, 297–313.

Spencer, J.R., Tamppari, L.K., Martin, T.Z., Travis, L.D., 1999. Temperatures on europa from galileo photopolarimeter-radiometer: nighttime thermal anomalies. Science 284, 1514–1516.

Stack, K., Milliken, R., 2015. Modeling near-infrared reflectance spectra of clay and sulfate mixtures and implications for mars. Icarus 250, 332–356.

Stephan, K., Ciarniello, M., Poch, O., Schmitt, B., Haack, D., Raponi, A., 2021. Vis-nir/swir spectral properties of h2o ice depending on particle size and surface temperature. Minerals 11, 1328.

Villanueva, G., Hammel, H., Milam, S., Faggi, S., Kofman, V., Roth, L., Hand, K., Paganini, L., Stansberry, J., Spencer, J., et al., 2023. Endogenous co2 ice mixture on the surface of europa and no detection of plume activity. Science 381, 1305–1308.

Yarnall, Y.Y., Hudson, R.L., 2022. Crystalline ices–densities and comparisons for planetary and interstellar applications. Icarus 373, 114799.